Letter | Editors' Suggestion | Featured in Physics

Contribution of negative-energy states to the $E2$-$M1$ polarizability of optical clocks

Fang-Fei Wu, Ting-Yun Shi, Wei-Tou Ni, and Li-Yan Tang*

State Key Laboratory of Magnetic Resonance and Atomic and Molecular Physics, Wuhan Institute of Physics and Mathematics, Innovation Academy for Precision Measurement Science and Technology, Chinese Academy of Sciences, Wuhan 430071, People's Republic of China

(Received 16 June 2023; accepted 19 September 2023; published 9 November 2023)

We investigate the contribution of negative-energy states on the $E2$ and $M1$ polarizabilities for the $^1S_0$ and $^3P_0$ states of the Sr clock and find that they dominate the $E2$-$M1$ polarizability difference. Our calculated result is $-7.74(3.92)\times10^{-5}$ a.u., which resolves the sign inconsistency between theory and experiment. Additionally, we extend our method to other optical clocks, confirming the crucial role of negative-energy states in determining the $M1$ polarizability.

DOI: 10.1103/PhysRevA.108.L051101

Introduction. Optical clocks have achieved an unprecedented level of stability, precision, and sensitivity [1–6], making them widely used to define the time of second, test the Einstein equivalence principle, and search for variations in the fundamental constants [6–12]. Further advancements in optical clock technology would enable new applications, such as the detection of gravitational waves in space using an astronomical unit-sized network [13–15].

Both atomic and ion optical clocks exhibit significant contributions from the ac Stark shift to the total clock uncertainty [1,16–22]. The accurate determination and theoretical understanding of the ac Stark shift are crucial for improving optical clocks. For an atom in a laser field, the energy levels shift due to the frequency-dependent polarizabilities [23]. To cancel the dominant electric dipole ($E1$) Stark shift, the optical clock operates at the magic wavelength [24,25]. However, as the precision of optical clocks approaches 10^{-18} or beyond, the contributions of electric quadrupole ($E2$) and magnetic dipole ($M1$) polarizabilities become significant [26–30].

For the Sr optical clock, the $E2$-$M1$ polarizability difference at the magic wavelength of 813.4280(5) nm [31] is inconsistent between the theory [26–28,32] and experiment [29,33,34], even the opposite in sign, as shown in Fig. 1. In 2018, Porsev *et al.* reported a value of $2.80(36)\times10^{-5}$ a.u. [$\sim$0.339(44) mHz] using the configuration interaction combined linearized coupled-cluster (CI+all-order) method [28]. Another result of $2.68(94)\times10^{-5}$ a.u. [$\sim$0.324(115) mHz] was obtained using the combined method of Dirac-Fock plus core polarization (DFCP) and relativistic configuration interaction (RCI) approaches [32]. Surprisingly, both of these theoretical results have opposite signs to the measured value of $-0.962(40)$ mHz by RIKEN [29], despite agreeing with each other. Recently, PTB and JILA reported independent experimental determinations of the $E2$-$M1$ polarizability difference of -987^{+174}_{-223} [33] μHz and $-1.24(5)$ mHz [34], respectively. Both experimental results have the same negative sign as the measurement by RIKEN, which further highlights the inconsistency between theory and experiment.

To accurately calculate the multipolar $E2$ and $M1$ polarizabilities using the sum-over-states method, it is crucial to maintain the completeness of the intermediate states. Therefore, in relativistic formalism, it is necessary to take into account the contribution of virtual electron-positron pairs in the intermediate states, i.e., the Dirac negative-energy-states (hole, virtual positron) contribution. The importance of this contribution has been studied in calculating the g factor of atomic systems [35–42]. Nevertheless, the contribution of negative-energy states to the dynamic multipolar polarizabilities $E2$ and $M1$ for optical clocks has not been previously investigated.

In this study, we take account of the contributions from negative-energy states to the dynamic multipolar polarizabilities using an improved DFCP+RCI method. Our findings indicate that, for the $M1$ polarizability, the contribution from negative-energy states is significantly larger than that of positive-energy states by several orders of magnitude. For the Sr clock, we determine the $E2$-$M1$ polarizability difference to be $-7.74(3.92)\times10^{-5}$ a.u. [$-0.935(477)$ mHz], which is consistent with all experimental results. Our research resolves the sign inconsistency for the $E2$-$M1$ polarizability difference between theory and experiment, and confirms the importance of negative-energy states for the $M1$ polarizability in optical clocks.

Theoretical Method. In comparison with existing calculations, we have developed a combined DFCP and RCI method that includes the negative-energy states. The implementation details are as follows.

First, the core-orbital wave functions $\psi(\boldsymbol{r})$ of the frozen core are obtained through a Dirac-Fock (DF) calculation [43]. These wave functions are then used to construct the DF potential $V_{\rm DF}(\boldsymbol{r})$ between a valence electron and the core.

Next, the monovalent-electron wave functions, consisting of two branches $\phi_+(\boldsymbol{r})$ and $\phi_-(\boldsymbol{r})$, corresponding to the wave functions of positive-energy and negative-energy states, are obtained by solving the following DFCP equation

$$h_{\rm DFCP}(\boldsymbol{r})\phi_\pm(\boldsymbol{r}) = \varepsilon\phi_\pm(\boldsymbol{r}), \tag{1}$$

*lytang@apm.ac.cn

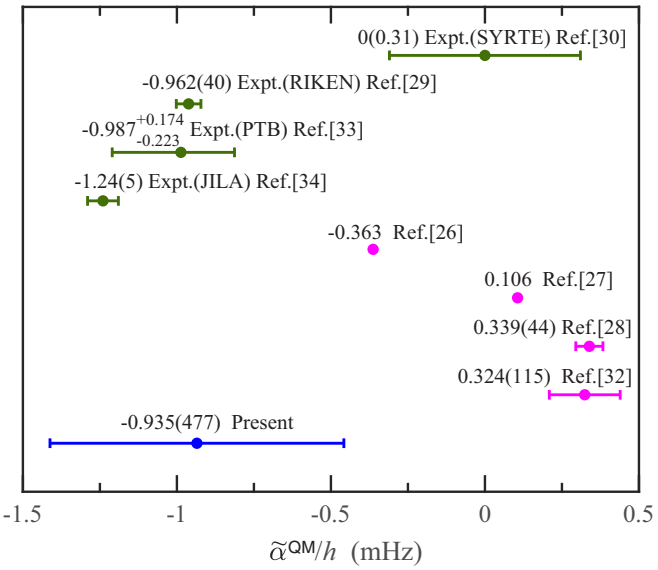

FIG. 1. Comparison of the $E2$-$M1$ polarizability difference $\tilde{\alpha}^{\mathrm{QM}}/h$ (in mHz) for the Sr clock. The green data points represent experimental results, the magenta data points represent other theoretical results, and the blue data point represents our present result.

where $h_{\mathrm{DFCP}}(\boldsymbol{r})$ represents the DFCP Hamiltonian

$$h_{\mathrm{DFCP}}(\boldsymbol{r}) = c\boldsymbol{\alpha}\cdot\mathbf{p} + (\beta-1)c^2 - \frac{Z}{r} + V_{\mathrm{DF}}(\boldsymbol{r}) + V_1(\boldsymbol{r}), \quad (2)$$

where $\boldsymbol{\alpha}$ and β are the 4×4 Dirac matrices, $\mathbf{p}$ is the momentum operator, and $V_1(\boldsymbol{r})$ is the one-body core-polarization potential [32,44].

For the monovalent-electron Mg^+, Ca^+, and Sr^+ ions investigated in this study, the first two steps are sufficient to obtain the fundamental structural information of the ions. However, for divalent-electron atoms such as Mg, Ca, Sr, and Cd, additional configuration interaction calculations are required. Utilizing the monovalent-electron ion wave functions $\phi_+(\boldsymbol{r})$ and $\phi_-(\boldsymbol{r})$ obtained in the second step, we construct the configuration-state wave functions $\Phi_I(\sigma\pi JM)$ based on three different combinations of $\{\phi_+(\boldsymbol{r}),\phi_+(\boldsymbol{r})\}$, $\{\phi_+(\boldsymbol{r}),\phi_-(\boldsymbol{r})\}$, and $\{\phi_-(\boldsymbol{r}),\phi_-(\boldsymbol{r})\}$, which establish a new configuration space for the calculations of divalent-electron atoms. Figure 2 illustrates the relationship between the positive-energy states and negative-energy states involved in the Sr clock. The wave function of divalent-electron atoms can be obtained by solving the following eigenequation:

$$\left[\sum_{i=1}^{2} h_{\mathrm{DFCP}}(\boldsymbol{r}_i) + \frac{1}{\boldsymbol{r}_{12}} + V_2(\boldsymbol{r}_{12})\right]|\Psi_\pm(\pi JM)\rangle = E|\Psi_\pm(\pi JM)\rangle, \quad (3)$$

where $V_2(\boldsymbol{r}_{12})$ represents the two-body core-polarization interaction [32,45,46].

The wave function $|\Psi_\pm(\pi JM)\rangle$ with parity π, angular momentum J, and magnetic quantum number M is likewise separated into two branches, namely, the positive-energy states $|\Psi_+(\pi JM)\rangle$ and the negative-energy states $|\Psi_-(\pi JM)\rangle$. These states can be expressed as a linear combination of the configuration-state wave functions

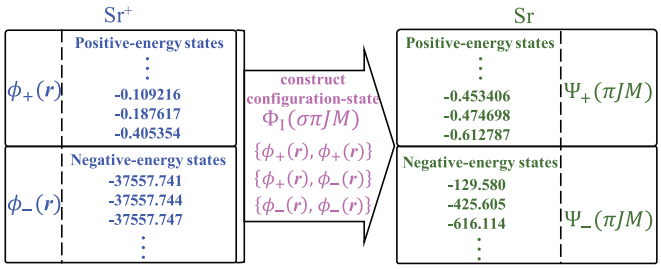

FIG. 2. Sketch diagram for obtaining the positive- and negative-energy states of the Sr clock. $\phi_+(\boldsymbol{r})$ and $\phi_-(\boldsymbol{r})$ represent two branches of the Sr^+ wave functions, which are used to construct the configuration state wavefunctions $\Phi_I(\sigma\pi JM)$. While $\Psi_+(\pi JM)$ and $\Psi_-(\pi JM)$ represent two branches of the Sr wave functions.

$$|\Psi_\pm(\pi JM)\rangle = \sum_I C_I|\Phi_I(\sigma\pi JM)\rangle, \quad (4)$$

where C_I and σ represent, respectively, the expansion coefficients and the additional quantum number that uniquely define each configuration state.

E2-M1 Polarizabilities. When a neutral atom or ion is exposed to a linearly polarized laser field with frequency ω, the dynamic $M1$ polarizability $\alpha^{M1}(\omega)$ for the initial state $|n_0J_0M_0\rangle$ (where n_0 represents all other quantum numbers) can be given by

$$\alpha^{M1}(\omega) = \alpha_S^{M1}(\omega) + g_2(J_0,M_0)\alpha_T^{M1}(\omega), \quad (5)$$

$$\alpha_S^{M1}(\omega) = \frac{2}{3(2J_0+1)}\sum_{n\pm}\frac{\Delta E_{n0}|\langle n_0J_0\|T_{M1}\|nJ_n\rangle|^2}{\Delta E_{n0}^2-\omega^2}, \quad (6)$$

$$\alpha_T^{M1}(\omega) = \sqrt{\frac{40J_0(2J_0-1)}{3(2J_0+3)(J_0+1)(2J_0+1)}}\sum_{n\pm}(-1)^{J_0+J_n} \times \begin{Bmatrix} 1 & 1 & 2 \\ J_0 & J_0 & J_n \end{Bmatrix}\frac{\Delta E_{n0}|\langle n_0J_0\|T_{M1}\|nJ_n\rangle|^2}{\Delta E_{n0}^2-\omega^2}, \quad (7)$$

and

$$g_2(J_0,M_0) = \frac{3M_0^2 - J_0(J_0+1)}{J_0(2J_0-1)}, \quad J_0 > \frac{1}{2}. \quad (8)$$

Here, $\alpha_S^{M1}(\omega)$ and $\alpha_T^{M1}(\omega)$ represent the scalar and tensor $M1$ polarizabilities, respectively. In Eqs. (6) and (7), T_{M1} denotes the $M1$ transition operator, while ΔE_{n0} is the transition energy between the initial state $|n_0J_0\rangle$ and the intermediate state $|nJ_n\rangle$. The summation index $n_\pm$ ranges over all positive-energy states and negative-energy states.

The general expression for the dynamic $E2$ polarizability of the initial state $|n_0J_0M_0\rangle$ can be written as

$$\alpha^{E2}(\omega) = \tfrac{1}{30}(\alpha\omega)^2\big[\alpha_S^{E2}(\omega) + g_2(J_0,M_0)\alpha_{T1}^{E2}(\omega) + g_4(J_0,M_0)\alpha_{T2}^{E2}(\omega)\big], \quad (9)$$

where the scalar and tensor $E2$ polarizabilities, denoted by $\alpha_S^{E2}(\omega)$, $\alpha_{T1}^{E2}(\omega)$, and $\alpha_{T2}^{E2}(\omega)$, are derived as follows:

$$\alpha_S^{E2}(\omega) = \frac{1}{(2J_0+1)} \sum_{n\pm} \frac{\Delta E_{n0} |\langle n_0 J_0 \| T_{E2} \| n J_n \rangle|^2}{\Delta E_{n0}^2 - \omega^2}, \tag{10}$$

$$\alpha_{T1}^{E2}(\omega) = 5\sqrt{\frac{10J_0(2J_0-1)}{7(2J_0+3)(J_0+1)(2J_0+1)}} \sum_{n\pm} (-1)^{J_0+J_n+1} \begin{Bmatrix} 2 & 2 & 2 \\ J_0 & J_0 & J_n \end{Bmatrix} \frac{\Delta E_{n0} |\langle n_0 J_0 \| T_{E2} \| n J_n \rangle|^2}{\Delta E_{n0}^2 - \omega^2}, \tag{11}$$

$$\alpha_{T2}^{E2}(\omega) = 9\sqrt{\frac{10J_0(J_0-1)(2J_0-1)(2J_0-3)}{7(2J_0+5)(2J_0+4)(2J_0+3)(2J_0+2)(2J_0+1)}} \sum_{n\pm} (-1)^{J_0+J_n} \begin{Bmatrix} 2 & 2 & 4 \\ J_0 & J_0 & J_n \end{Bmatrix} \frac{\Delta E_{n0} |\langle n_0 J_0 \| T_{E2} \| n J_n \rangle|^2}{\Delta E_{n0}^2 - \omega^2}, \tag{12}$$

T_{E2} in Eqs. (10) to (12) represents the $E2$ transition operator. $g_4(J_0, M_0)$ in Eq. (9) is expressed as

$$g_4(J_0, M_0) = \frac{3\left(5M_0^2 - J_0^2 - 2J_0\right)\left(5M_0^2 + 1 - J_0^2\right)}{J_0(J_0-1)(2J_0-1)(2J_0-3)} - \frac{10M_0^2\left(4M_0^2-1\right)}{J_0(J_0-1)(2J_0-1)(2J_0-3)}, \quad J_0 > \frac{3}{2}. \tag{13}$$

The reduced matrix elements $\langle n_0 J_0 \| T_{M1} \| n J_n \rangle$ and $\langle n_0 J_0 \| T_{E2} \| n J_n \rangle$ can be expressed in terms of the reduced matrix elements $\langle i \| t_{M1} \| k \rangle$ and $\langle i \| t_{E2} \| k \rangle$ of the corresponding monovalent-electron system [47]

$$\langle i \| t_{M1} \| j \rangle = \frac{\kappa_i + \kappa_j}{2} \langle -\kappa_i \| C^1 \| \kappa_j \rangle \int r [P_i(r) Q_j(r) + Q_i(r) P_j(r)] dr, \tag{14}$$

$$\langle i \| t_{E2} \| j \rangle = \langle \kappa_i \| C^2 \| \kappa_j \rangle \int r^2 [P_i(r) P_j(r) + Q_i(r) Q_j(r)] dr, \tag{15}$$

where $P_i(r)$ and $Q_i(r)$ denote the large and small components of the wave functions for the corresponding monovalent-electron system.

Results and Discussions. By utilizing the improved DFCP + RCI approach that includes negative-energy states, we performed comprehensive calculations of the dynamic multipolar polarizabilities for the developing atomic clocks.

Tables I and II present the itemized contributions of the dynamic $E2$ and $M1$ polarizabilities, respectively, at the 813.4280(5)-nm magic wavelength [31] of the Sr clock. For the $E2$ polarizability, the core contribution is 4.38×10^{-8} a.u. and the negative-energy state contribution is less than 10^{-14} for both the $5s^2\ ^1S_0$ and $5s5p\ ^3P_0^o$ clock states. Hence, both of these contributions can be neglected. However, the negative-energy states have a significant impact on the dynamic $M1$ polarizability. With the inclusion of negative-energy states, the dynamic $M1$ polarizability at the 813.4280(5)-nm magic wavelength for the $5s^2\ ^1S_0$ state changes from 2.17×10^{-9} a.u. to -6.18×10^{-4} a.u. Similarly, for the $5s5p\ ^3P_0^o$ state, the contribution of negative-energy states accounts for 99% of the $M1$ polarizability. These results include the core contribution of -2.335×10^{-4} a.u. [48] to the dynamic $M1$ polarizability.

To investigate the primary reason for the large contribution of negative-energy states, we performed a detailed analysis of the contribution. Our findings indicate that, unlike the

TABLE I. Itemized contributions (Contr.) of the dynamic $E2$ polarizability (in a.u.) at the 813.4280(5)-nm magic wavelength of the Sr clock. Tail represents the contribution from other positive-energy states, while α^{E2+} and α^{E2-} represent the total contribution from positive-energy and negative-energy states, respectively. The numbers in the square brackets denote powers of ten.

$5s^2\ ^1S_0$		$5s5p\ ^3P_0^o$	
Sub item	Contr.	Sub item	Contr.
$5s4d\ ^3D_2$	1.258[−7]	$5s5p\ ^3P_2^o$	−2.805[−6]
$5s4d\ ^1D_2$	6.965[−5]	$5d5p\ ^3F_2^o$	3.095[−5]
$5s5d\ ^1D_2$	1.224[−5]	$5d5p\ ^1D_2^o$	3.149[−6]
$5s5d\ ^3D_2$	1.106[−8]	$5s6p\ ^3P_2^o$	1.741[−5]
$5p^2\ ^3P_2$	5.966[−8]	$4d5p\ ^3D_2^o$	3.603[−6]
$5d^2\ ^1D_2$	3.887[−8]	$5d5p\ ^3P_2^o$	2.139[−6]
$5s6d\ ^3D_2$	4.981[−10]	$5s4f\ ^3F_2^o$	2.644[−5]
$5s6d\ ^1D_2$	1.226[−7]	$5s7p\ ^3P_2^o$	2.601[−6]
$5s7d\ ^1D_2$	2.600[−6]	$5s5f\ ^3F_2^o$	8.768[−6]
Tail	7.950[−6]	Tail	3.214[−5]
α^{E2+}	9.28[−5]	α^{E2+}	12.44[−5]
α^{E2-}	−8.64[−16]	α^{E2-}	−1.10[−15]
Total	9.28[−5]	Total	12.44[−5]

TABLE II. Itemized contributions (Contr.) of the dynamic $M1$ polarizability (in a.u.) at the 813.4280(5)-nm magic wavelength of the Sr clock. Tail represents the contribution from other positive-energy states, while α^{M1+} and α^{M1-} represent the total contribution from positive-energy and negative-energy states, respectively. The numbers in the square brackets denote powers of ten.

$5s^2\ ^1S_0$		$5s5p\ ^3P_0^o$	
Sub item	Contr.	Sub item	Contr.
$5s4d\ ^3D_1$	1.483[−15]	$5s5p\ ^3P_1^o$	−4.811[−6]
$5s6s\ ^3S_1$	4.098[−13]	$5s5p\ ^1P_1^o$	−2.702[−7]
$5s5d\ ^3D_1$	1.273[−12]	$5s6p\ ^3P_1^o$	7.336[−10]
$5p^2\ ^3P_1$	1.539[−9]	$5s6p\ ^1P_1^o$	1.766[−8]
Tail	5.81[−10]	Tail	1.35[−8]
α^{M1+}	2.17[−9]	α^{M1+}	−5.05[−6]
α^{M1-}	−6.18[−4]	α^{M1-}	−7.22[−4]
Total	−6.18[−4]	Total	−7.27[−4]

TABLE III. Dynamic $E2$ and $M1$ polarizabilities (in a.u.) at the 813.4280(5)-nm magic wavelength of the Sr clock. $\Delta\alpha^{E2}(\omega)$ and $\Delta\alpha^{M1}(\omega)$ are the dynamic $E2$ and $M1$ polarizability difference, respectively, and $\Delta\alpha^{\rm QM}(\omega) = \Delta\alpha^{M1}(\omega) + \Delta\alpha^{E2}(\omega)$. The numbers in parentheses represent the theoretical uncertainties, while the numbers in the square brackets denote powers of ten.

Polarizability	Present	Ref. [32]	Ref. [28]
$\alpha^{E2}_{^1S_0}(\omega)$	9.28(57)[−5]	9.26(56)[−5]	8.87(26)[−5]
$\alpha^{E2}_{^3P^o_0}(\omega)$	12.44(76)[−5]	12.44(76)[−5]	12.2(25)[−5]
$\Delta\alpha^{E2}(\omega)$	3.16(95)[−5]	3.18(94)[−5]	3.31(36)[−5]
$\alpha^{M1}_{^1S_0}(\omega)$	−6.18(24)[−4]	2.12(13)[-9]	2.37[-9]
$\alpha^{M1}_{^3P^o_0}(\omega)$	−7.27(30)[−4]	−5.05(31)[−6]	−5.08[−6]
$\Delta\alpha^{M1}(\omega)$	−1.09(38)[−4]	−5.05(31)[−6]	−5.08[−6]
$\Delta\alpha^{\rm QM}(\omega)$	−7.74(3.92)[−5]	2.68(94)[−5]	2.80(36)[−5]

positive-energy states, the contribution from negative-energy states does not originate primarily from a few intermediate states but rather from a cumulative effect of numerous states with energies ranging from −37559 a.u. to −37557 a.u. ($2mc^2 \approx 37558$ a.u.). Although these negative-energy states are far removed from the initial state, their radial wave functions $Q_j(r)$ exhibit significant overlap with the $P_i(r)$ component of the initial state wave function, leading to a large $P_i(r)Q_j(r)$ product in Eq. (14). In other words, it is a series of significant $M1$ transition matrix elements between the negative-energy states and the initial state that results in the dominant contribution of negative-energy states to the $M1$ polarizability.

Since the values obtained using the DFCP + RCI method for the $E1$ polarizability of the Sr, Mg, and Cd clocks agree with the results of the CI+all-order method within 3% [32,49,50], we conservatively assign an error of 3% to all the reduced matrix elements to evaluate the uncertainty of present $E2$ and $M1$ polarizabilities. The results, along with a detailed comparison of the Sr clock, are summarized in Table III. The present $E2$ polarizability is in good agreement with the results reported in previous investigations [28,32], which only considered the contribution of positive-energy states. In contrast, the value of the $M1$ polarizability $\Delta\alpha^{M1}(\omega)$ obtained in this study is two orders of magnitude larger than the values reported in Refs. [28,32], primarily due to the dominant contribution of negative-energy states. By adding $\Delta\alpha^{M1}(\omega)$ and $\Delta\alpha^{E2}(\omega)$, we obtain the $E2$-$M1$ polarizability difference $\Delta\alpha^{\rm QM}(\omega) = -7.74(3.92)\times10^{-5}$ a.u. for the Sr clock. The large uncertainty of present result is due to the cancellation of significant digits when two terms are added together.

To facilitate a direct comparison with the experimental results of the Sr clock, we convert all the theoretical values of $\Delta\alpha^{\rm QM}(\omega)$ from a.u. to Hz using the formula $\tilde{\alpha}^{\rm QM} = \Delta\alpha^{\rm QM}(\omega)E_R/\alpha^{E1}(\omega)$, where $\alpha^{E1}(\omega) = 287(17)$ a.u. is the present dynamic $E1$ polarizability at the magic wavelength of 813.4280(5) nm [31], and E_R is the lattice photon recoil energy [29]. The comparison is presented in Fig. 1. The uncertainty of theoretical values for $\tilde{\alpha}^{\rm QM}/h$ is obtained by using error propagation theory. Our value of −0.935(477) mHz is in agreement with the three measured results of −0.962(40) [29], $-0.987^{+0.174}_{-0.223}$ [33], and −1.24(5) mHz [34]. This demonstrates the importance of including negative-energy states in the determination of multipolar polarizabilities of the Sr clock. However, there is a discrepancy between the measurement of JILA [34] and that of RIKEN [29], which urgently requires higher-accuracy theoretical calculation or experimental measurement to resolve it.

TABLE IV. Dynamic $E2$ polarizabilities (in a.u.) at the magic wavelengths λ_m (in nm) for the Mg, Ca, Cd, Mg^+, Ca^+, and Sr^+ clocks. $\Delta\alpha^{E2}(\omega)$ represents the dynamic $E2$ polarizability difference. The contribution of negative-energy states is less than 10^{-15} and can be safely neglected in our calculations. The numbers in parentheses indicate the theoretical uncertainties, while the numbers in square brackets represent powers of ten.

System	λ_m(nm)	$\alpha^{E2}_{^1S_0}(\omega)$	$\alpha^{E2}_{^3P^o_0}(\omega)$	$\Delta\alpha^{E2}(\omega)$
Mg	468.46(21)[a]	4.25(26)[−5]	1.02(6)[−4]	5.95(65)[−5]
Ca	735.5(20)[b]	7.51(44)[−5]	1.00(6)[−4]	2.49(48)[−5]
Cd	419.88(14)[c]	2.53(15)[−5]	9.91(60)[−5]	7.38(62)[−5]
		$\alpha^{E2}_{^2S_{1/2}}(\omega)$	$\alpha^{E2}_{^2D_{5/2}}(\omega)$	$\Delta\alpha^{E2}(\omega)$
Mg^+	737	2.73(17)[−6]	4.54(28)[−5]	4.27(28)[−5]
Ca^+	1056.37(9)[d]	1.14(7)[−5]	6.80(38)[−7]	−1.07(7)[−5]
Sr^+	1898	3.83(23)[−6]	5.13(29)[−7]	−3.32(23)[−6]

[a]Ref. [51]; [b]Ref. [52]; [c]Ref. [53]; [d]Ref. [56].

Furthermore, we apply the present method to calculate the dynamic $E2$ and $M1$ polarizabilities of various other optical clocks, and present the results in Tables IV and V. For the Mg, Ca, and Cd atomic clocks, we calculate the values at the measured magic wavelengths [51–53]. For the Mg^+, Ca^+, and Sr^+ ion clocks, we compute the values at the magic wavelengths that are far from resonance, as all-optical trapping of ions with these wavelengths can effectively suppress micromotion and ac Stark shift, and improve the frequency stability of clocks [54–56]. Based on detailed comparison of the reduced matrix

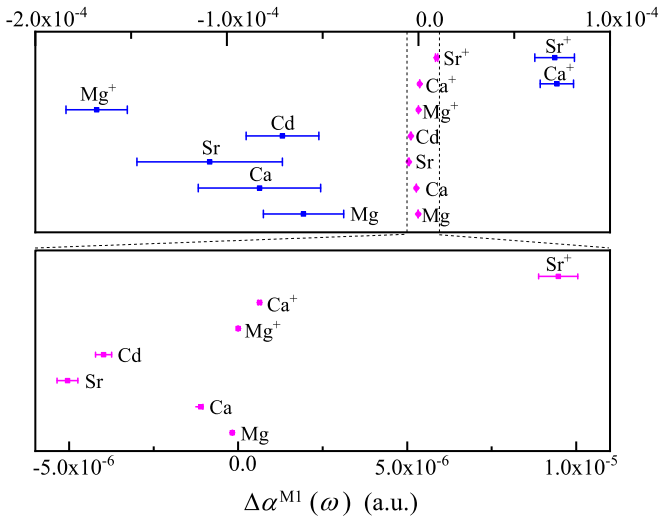

FIG. 3. Comparison of the $M1$ polarizability difference $\Delta\alpha^{M1}(\omega)$ (in a.u.) for other optical clocks. The blue and magenta lines represent $\Delta\alpha^{M1}(\omega)$ with and without the contribution of negative-energy states, respectively.

TABLE V. Dynamic $M1$ polarizabilities (in a.u.) at the magic wavelengths λ_m (in nm) for the Mg, Ca, Cd, Mg^+, Ca^+, and Sr^+ clocks. The values of $\alpha^{M1\pm}(\omega)$ and $\alpha^{M1+}(\omega)$ represent the dynamic $M1$ polarizability with and without the contribution of negative-energy states, respectively. $\Delta\alpha^{M1\pm}(\omega)$ and $\Delta\alpha^{M1+}(\omega)$ represent the dynamic $M1$ polarizability difference with and without the contribution of negative-energy states, respectively. The numbers in parentheses indicate the theoretical uncertainties, while the numbers in square brackets represent powers of ten.

System	λ_m(nm)	$\alpha^{M1+}_{^1S_0}(\omega)$	$\alpha^{M1\pm}_{^1S_0}(\omega)$	$\alpha^{M1+}_{^3P^o_0}(\omega)$	$\alpha^{M1\pm}_{^3P^o_0}(\omega)$	$\Delta\alpha^{M1+}(\omega)$	$\Delta\alpha^{M1\pm}(\omega)$
Mg	468.46(21)[a]	1.23(7)[−11]	−2.49(13)[−4]	−1.72(10)[−7]	−3.09(16)[−4]	−1.72(10)[−7]	−0.60(21)[−4]
Ca	735.5(20)[b]	4.69(29)[−10]	−4.67(20)[−4]	−1.11(7)[−6]	−5.50(25)[−4]	−1.11(7)[−6]	−0.83(32)[−4]
Cd	419.88(14)[c]	1.45(9)[−9]	−4.40(11)[−4]	−3.98(24)[−6]	−5.11(15)[−4]	−3.98(24)[−6]	−0.71(19)[−4]
		$\alpha^{M1+}_{^2S_{1/2}}(\omega)$	$\alpha^{M1\pm}_{^2S_{1/2}}(\omega)$	$\alpha^{M1+}_{^2D_{5/2}}(\omega)$	$\alpha^{M1\pm}_{^2D_{5/2}}(\omega)$	$\Delta\alpha^{M1+}(\omega)$	$\Delta\alpha^{M1\pm}(\omega)$
Mg^+	737	2.15(13)[−13]	−1.21(5)[−4]	−4.35(26)[−9]	−2.89(15)[−4]	−4.35(26)[−9]	−1.68(16)[−4]
Ca^+	1056.37(9)[d]	2.75(17)[−13]	−2.67(8)[−4]	6.33(39)[−7]	−1.95(4)[−4]	6.33(39)[−7]	0.72(9)[−4]
Sr^+	1898	4.64(28)[−13]	−3.86(9)[−4]	9.47(58)[−6]	−3.15(5)[−4]	9.47(58)[−6]	0.71(10)[−4]

[a]Ref. [51]; [b]Ref. [52]; [c]Ref. [53]; [d]Ref. [56].

elements with other available results, we also introduce 3% fluctuation into all the reduced matrix elements to conservatively estimate the uncertainties of $M1$ and $E2$ polarizabilities for other clocks.

Similar to the Sr clock, the results for all the other clocks in Tables IV and V indicate that the negative-energy states have a negligible impact on the $E2$ polarizability, but have a significant contribution to the $M1$ polarizability. The intuitive comparison of the $M1$ polarizability difference with and without the negative-energy states is shown in Fig. 3. For each clock, the value in blue deviates significantly from the value in magenta, demonstrating the importance of the negative-energy-states contribution.

Conclusion. Motivated by the sign inconsistency between existing theory and experiment in the $E2$-$M1$ polarizability difference of the Sr clock, we developed a combined DFCP+RCI method that includes negative-energy states and applied it to comprehensively calculate the dynamic $M1$ and $E2$ polarizabilities for current developing clocks. Our calculation shows that the $E2$-$M1$ polarizability difference in the Sr clock is $-7.74(3.92)\times10^{-5}$ a.u., which is consistent in sign with all the measured values. Moreover, we found that the contribution of negative-energy states to the $M1$ polarizability is also crucial for other optical clocks. Therefore, our work has resolved the sign inconsistency for the $E2$-$M1$ polarizability difference in the Sr clock, and further emphasizes the importance of negative-energy states in evaluating the multipolar interaction between light and matter in precision measurement physics.

Acknowledgments. We thank Y.-H. Zhang and J. Jiang for valuable discussions on negative-energy states, in addition we thank Z.-C. Yan, J. Chen, K.-L. Gao, B.-L. Lü, and X.-Q. Qi for their valuable suggestions on the manuscript. This work was supported by the National Natural Science Foundation of China under Grants No. 12174402, No. 12274423, No. 12004124, and No. 12121004, as well as the Nature Science Foundation of Hubei Province under Grants No. 2019CFA058 and No. 2022CFA013.

[1] S. M. Brewer, J.-S. Chen, A. M. Hankin, E. R. Clements, C. W. Chou, D. J. Wineland, D. B. Hume, and D. R. Leibrandt, $^{27}Al^+$ Quantum-Logic Clock with a Systematic Uncertainty Below 10^{-18}, Phys. Rev. Lett. **123**, 033201 (2019).

[2] C. Sanner, N. Huntemann, R. Lange, C. Tamm, E. Peik, M. S. Safronova, and S. G. Porsev, Optical clock comparison for Lorentz symmetry testing, Nature (London) **567**, 204 (2019).

[3] B. M. Roberts, P. Delva, A. Al-Masoudi, A. Amy-Klein, C. Brentsen, C. F. A. Baynham, E. Benkler, S. Bilicki, S. Bize, W. Bowden *et al.*, Search for transient variations of the fine structure constant and dark matter using fiber-linked optical atomic clocks, New J. Phys. **22**, 093010 (2020).

[4] R. Lange, N. Huntemann, J. M. Rahm, C. Sanner, H. Shao, B. Lipphardt, C. Tamm, S. Weyers, and E. Peik, Improved Limits for Violations of Local Position Invariance from Atomic Clock Comparisons, Phys. Rev. Lett. **126**, 011102 (2021).

[5] K. Beloy, M. I. Bodine, T. Bothwell, S. M. Brewer, S. L. Bromley, J.-S. Chen, J.-D. Deschênes, S. A. Diddams, R. J. Fasano, T. M. Fortier *et al.*, Frequency ratio measurements at 18-digit accuracy using an optical clock network, Nature (London) **591**, 564 (2021).

[6] T. Bothwell, C. J. Kennedy, A. Aeppli, D. Kedar, J. M. Robinson, E. Oelker, A. Staron, and J. Ye, Resolving the gravitational redshift across a millimetre-scale atomic sample, Nature (London) **602**, 420 (2022).

[7] F. Bregolin, G. Milani, M. Pizzocaro, B. Rauf, P. Thoumany, F. Levi, and D. Calonico, Optical lattice clocks towards the redefinition of the second, J. Phys.: Conf. Ser. **841**, 012015 (2017).

[8] K. Yamanaka, N. Ohmae, I. Ushijima, M. Takamoto, and H. Katori, Frequency Ratio of ^{199}Hg and ^{87}Sr Optical Lattice Clocks Beyond the SI Limit, Phys. Rev. Lett. **114**, 230801 (2015).

[9] A. D. Ludlow, M. M. Boyd, J. Ye, E. Peik, and P. O. Schmidt, Optical atomic clocks, Rev. Mod. Phys. **87**, 637 (2015).

[10] R. M. Godun, P. B. R. Nisbet-Jones, J. M. Jones, S. A. King, L. A. M. Johnson, H. S. Margolis, K. Szymaniec, S. N. Lea, K. Bongs, and P. Gill, Frequency Ratio of Two Optical Clock Transitions in $^{171}Yb^+$ and Constraints on the Time Variation of Fundamental Constants, Phys. Rev. Lett. **113**, 210801 (2014).

[11] N. Huntemann, B. Lipphardt, C. Tamm, V. Gerginov, S. Weyers, and E. Peik, Improved Limit on a Temporal Variation of m_p/m_e

from Comparisons of Yb^+ and Cs Atomic Clocks, Phys. Rev. Lett. **113**, 210802 (2014).

[12] M. S. Safronova, S. G. Porsev, C. Sanner, and J. Ye, Two Clock Transitions in Neutral Yb for the Highest Sensitivity to Variations of the Fine-Structure Constant, Phys. Rev. Lett. **120**, 173001 (2018).

[13] S. Kolkowitz, I. Pikovski, N. Langellier, M. D. Lukin, R. L. Walsworth, and J. Ye, Gravitational wave detection with optical lattice atomic clocks, Phys. Rev. D **94**, 124043 (2016).

[14] T. Ebisuzaki, H. Katori, J. Makino, A. Noda, H. Shinkai, and T. Tamagawa, INO: Interplanetary network of optical lattice clocks, Int. J. Mod. Phys. D **29**, 1940002 (2020).

[15] W.-T. Ni, Gravitational wave detection in space, Int. J. Mod. Phys. D **25**, 1630001 (2016).

[16] T. Nicholson, S. Campbell, R. Hutson, G. Marti, B. Bloom, R. McNally, W. Zhang, M. Barrett, M. Safronova, G. Strouse *et al.*, Systematic evaluation of an atomic clock at 2×10^{-18} total uncertainty, Nat. Commun. **6**, 6896 (2015).

[17] I. Ushijima, M. Takamoto, M. Das, T. Ohkubo, and H. Katori, Cryogenic optical lattice clocks, Nat. Photon. **9**, 185 (2015).

[18] W. F. McGrew, X. Zhang, R. J. Fasano, S. A. Schäffer, K. Beloy, D. Nicolodi, R. C. Brown, N. Hinkley, G. Milani, M. Schioppo, T. H. Yoon, and A. D. Ludlow, Atomic clock performance beyond the geodetic limit, Nature (London) **564**, 87 (2018).

[19] T. Bothwell, D. Kedar, E. Oelker, J. M. Robinson, S. L. Bromley, W. L. Tew, J. Ye, and C. J. Kennedy, JILA SrI optical lattice clock with uncertainty of 2×10^{-18}, Metrologia **56**, 065004 (2019).

[20] E. Oelker, R. B. Hutson, C. J. Kennedy, L. Sonderhouse, T. Bothwell, A. Goban, D. Kedar, C. Sanner, J. M. Robinson, G. E. Marti *et al.*, Demonstration of 4.8×10^{-17} stability at 1s for two independent optical clocks, Nat. Photon. **13**, 714 (2019).

[21] B.-K. Lu, Z. Sun, T. Yang, Y.-G. Lin, Q. Wang, Y. Li, F. Meng, B.-K. Lin, T.-C. Li, and Z.-J. Fang, Improved evaluation of BBR and collisional frequency shifts of NIM-Sr2 with 7.2×10^{-18} total uncertainty, Chin. Phys. Lett. **39**, 080601 (2022).

[22] Y. Huang, B. Zhang, M. Zeng, Y. Hao, Z. Ma, H. Zhang, H. Guan, Z. Chen, M. Wang, and K. Gao, Liquid-Nitrogen-Cooled Ca^+ Optical Clock with Systematic Uncertainty of 3×10^{-18}, Phys. Rev. Appl. **17**, 034041 (2022).

[23] N. L. Manakov, V. D. Ovsiannikov, and L. P. Rapoport, *Atoms in a Laser Field* (North-Holland, Amsterdam, 1986).

[24] M. Takamoto, F.-L. Hong, R. Higashi, and H. Katori, An optical lattice clock, Nature (London) **435**, 321 (2005).

[25] A. D. Ludlow, M. M. Boyd, T. Zelevinsky, S. M. Foreman, S. Blatt, M. Notcutt, T. Ido, and J. Ye, Systematic Study of the ^{87}Sr Clock Transition in an Optical Lattice, Phys. Rev. Lett. **96**, 033003 (2006).

[26] V. D. Ovsiannikov, V. G. Pal'chikov, A. V. Taichenachev, V. I. Yudin, and H. Katori, Multipole, nonlinear, and anharmonic uncertainties of clocks of Sr atoms in an optical lattice, Phys. Rev. A **88**, 013405 (2013).

[27] H. Katori, V. D. Ovsiannikov, S. I. Marmo, and V. G. Palchikov, Strategies for reducing the light shift in atomic clocks, Phys. Rev. A **91**, 052503 (2015).

[28] S. G. Porsev, M. S. Safronova, U. I. Safronova, and M. G. Kozlov, Multipolar Polarizabilities and Hyperpolarizabilities in the Sr Optical Lattice Clock, Phys. Rev. Lett. **120**, 063204 (2018).

[29] I. Ushijima, M. Takamoto, and H. Katori, Operational Magic Intensity for Sr Optical Lattice Clocks, Phys. Rev. Lett. **121**, 263202 (2018).

[30] P. G. Westergaard, J. Lodewyck, L. Lorini, A. Lecallier, E. A. Burt, M. Zawada, J. Millo, and P. Lemonde, Lattice-Induced Frequency Shifts in Sr Optical Lattice Clocks at the 10^{-17} Level, Phys. Rev. Lett. **106**, 210801 (2011).

[31] J. Ye, H. J. Kimble, and H. Katori, Quantum state engineering and precision metrology using state-insensitive light traps, Science **320**, 1734 (2008).

[32] F.-F. Wu, Y.-B. Tang, T.-Y. Shi, and L.-Y. Tang, Dynamic multipolar polarizabilities and hyperpolarizabilities of the Sr lattice clock, Phys. Rev. A **100**, 042514 (2019).

[33] S. Dörscher, J. Klose, S. Maratha Palli, and C. Lisdat, Experimental determination of the $E2-M1$ polarizability of the strontium clock transition, Phys. Rev. Res. **5**, L012013 (2023).

[34] K. Kim, A. Aeppli, T. Bothwell, and J. Ye, Evaluation of Lattice Light Shift at Mid 10^{-19} Uncertainty for a Shallow Lattice Sr Optical Clock, Phys. Rev. Lett. **130**, 113203 (2023).

[35] V. M. Shabaev, D. A. Glazov, M. B. Shabaeva, V. A. Yerokhin, G. Plunien, and G. Soff, g factor of high-Z lithiumlike ions, Phys. Rev. A **65**, 062104 (2002).

[36] E. Lindroth and A. Ynnerman, *Ab initio* calculations of g_j factors for Li, Be^+, and Ba^+, Phys. Rev. A **47**, 961 (1993).

[37] D. A. Glazov, V. M. Shabaev, I. I. Tupitsyn, A. V. Volotka, V. A. Yerokhin, G. Plunien, and G. Soff, Relativistic and QED corrections to the g factor of Li-like ions, Phys. Rev. A **70**, 062104 (2004).

[38] A. Wagner, S. Sturm, F. Köhler, D. A. Glazov, A. V. Volotka, G. Plunien, W. Quint, G. Werth, V. M. Shabaev, and K. Blaum, g Factor of Lithiumlike Silicon $^{28}Si^{11+}$, Phys. Rev. Lett. **110**, 033003 (2013).

[39] V. A. Agababaev, D. A. Glazov, A. V. Volotka, D. V. Zinenko, V. M. Shabaev, and G. Plunien, Ground-state g factor of middle-Z boronlike ions, J. Phys.: Conf. Ser. **1138**, 012003 (2018).

[40] I. Arapoglou, A. Egl, M. Höcker, T. Sailer, B. Tu, A. Weigel, R. Wolf, H. Cakir, V. A. Yerokhin, N. S. Oreshkina *et al.*, g Factor of Boronlike Argon $^{40}Ar^{13+}$, Phys. Rev. Lett. **122**, 253001 (2019).

[41] H. Cakir, V. A. Yerokhin, N. S. Oreshkina, B. Sikora, I. I. Tupitsyn, C. H. Keitel, and Z. Harman, QED corrections to the g factor of Li- and B-like ions, Phys. Rev. A **101**, 062513 (2020).

[42] L. Wu, J. Jiang, Z.-W. Wu, Y.-J. Cheng, G. Gaigalas, and C.-Z. Dong, Energy levels, absorption oscillator strengths, transition probabilities, polarizabilities, and g factors of Ar^{13+} ions, Phys. Rev. A **106**, 012810 (2022).

[43] Y.-B. Tang, H.-X. Qiao, T.-Y. Shi, and J. Mitroy, Dynamic polarizabilities for the low-lying states of Ca^+, Phys. Rev. A **87**, 042517 (2013).

[44] J. Mitroy and D. W. Norcross, Electron-impact excitation of the resonance transition in Be^+, Phys. Rev. A **37**, 3755 (1988).

[45] J. Mitroy, M. S. Safronova, and C. W. Clark, Theory and applications of atomic and ionic polarizabilities, J. Phys. B: At. Mol. Opt. Phys. **43**, 202001 (2010).

[46] J. Mitroy and M. W. J. Bromley, Semi-empirical calculation of van der Waals coefficients for alkali-metal and alkaline-earth-metal atoms, Phys. Rev. A **68**, 052714 (2003).

[47] W. R. Johnson, *Atomic Structure Theory: Lectures on Atomic Physics* (Springer, Berlin, 2007).

[48] W. R. Johnson, D. Kolb, and K. Huang, Electric-dipole, quadrupole, and magnetic-dipole susceptibilities and shielding factors for closed-shell ions of the He, Ne, Ar, Ni, Cu^+, Kr, Pb, and Xe isoelectronic sequences, At. Data Nucl. Data Tables **28**, 333 (1983).

[49] F.-F. Wu, Y.-B. Tang, T.-Y. Shi, and L.-Y. Tang, Magic-intensity trapping of the Mg lattice clock with light shift suppressed below 10^{-19}, Phys. Rev. A **101**, 053414 (2020).

[50] M. Zhou and L.-Y. Tang, Calculations of dynamic multipolar polarizabilities of the Cd clock transition levels, Chin. Phys. B **30**, 083102 (2021).

[51] A. P. Kulosa, D. Fim, K. H. Zipfel, S. Rühmann, S. Sauer, N. Jha, K. Gibble, W. Ertmer, E. M. Rasel, M. S. Safronova, U. I. Safronova, and S. G. Porsev, Towards a Mg Lattice Clock: Observation of the $^1S_0 - {}^3P_0$ Transition and Determination of the Magic Wavelength, Phys. Rev. Lett. **115**, 240801 (2015).

[52] C. Degenhardt, H. Stoehr, U. Sterr, F. Riehle, and C. Lisdat, Wavelength-dependent ac Stark shift of the $^1S_0$ - $^3P_1$ transition at 657 nm in Ca, Phys. Rev. A **70**, 023414 (2004).

[53] A. Yamaguchi, M. S. Safronova, K. Gibble, and H. Katori, Narrow-line Cooling and Determination of the Magic Wavelength of Cd, Phys. Rev. Lett. **123**, 113201 (2019).

[54] P. Liu, Y. Huang, W. Bian, H. Shao, H. Guan, Y. Tang, C. Li, J. Mitroy, and K. Gao, Measurement of Magic Wavelengths for the $^{40}Ca^+$ Clock Transition, Phys. Rev. Lett. **114**, 223001 (2015).

[55] M. Enderlein, T. Huber, C. Schneider, and T. Schaetz, Single Ions Trapped in a One-Dimensional Optical Lattice, Phys. Rev. Lett. **109**, 233004 (2012).

[56] Y. Huang, H. Guan, C. Li, H. Zhang, B. Zhang, M. Wang, L. Tang, T. Shi, and K. Gao, Measurement of infrared magic wavelength for an all-optical trapping of $^{40}Ca^+$ ion clock, arXiv:2202.07828.